ORNL/SPR-2024/3302

Report: Automated Model for Improved Mapping of Country-Scale High-Resolution Coastal Bathymetry

Matt McCarthy
Dariusz Stramski
David Hughes
Rick Reynolds
Ishan Joshi

March 2024

DOCUMENT AVAILABILITY

Online Access: US Department of Energy (DOE) reports produced after 1991 and a growing number of pre-1991 documents are available free via https://www.osti.gov.

The public may also search the National Technical Information Service's National Technical Reports Library (NTRL) for reports not available in digital format.

DOE and DOE contractors should contact DOE's Office of Scientific and Technical Information (OSTI) for reports not currently available in digital format:

US Department of Energy
Office of Scientific and Technical Information
PO Box 62
Oak Ridge, TN 37831-0062
Telephone: (865) 576-8401
Fax: (865) 576-5728
Email: reports@osti.gov
Website: www.osti.gov

ORNL/SPR-2024/3302

Geospatial Science and Human Security Division

AUTOMATED MODEL FOR IMPROVED MAPPING OF COUNTRY-SCALE HIGH-RESOLUTION COASTAL BATHYMETRY

Matt J. McCarthy
Dariusz Stramski
David Hughes
Rick A. Reynolds
Ishan D. Joshi

March 2024

Prepared by
OAK RIDGE NATIONAL LABORATORY
Oak Ridge, TN 37831
managed by
UT-BATTELLE LLC
for the
US DEPARTMENT OF ENERGY
under contract DE-AC05-00OR22725

Contents

ABSTRACT

Accurate and up-to-date maps of coastal bathymetry are critical for a variety of sectors from vessel navigation to port construction and are increasingly vital to inform coastal infrastructure management amid accelerating sea-level rise and more frequent and severe storm-surge events. The primary challenges to accurate and efficient bathymetric mapping from optical remote sensing are: accurately modeling light attenuation in both the atmosphere and water column; and inefficient data processing pipelines for high-resolution satellite imagery. To address the effects of light attenuation within the water-column we have developed a novel physics-based bathymetry model that accounts for variations in water-column inherent optical properties on a pixel-by-pixel basis in optically-shallow aquatic environments, which represents a major advancement. For applications to satellite imagery, we have developed a software package that automatically applies the robust 6S atmospheric correction algorithm, estimates the bottom depth from the physics-based bathymetry model, which corrects for attenuation by suspended particulate matter and colored dissolved organic matter in the water column on a pixel-by-pixel basis, and leverages high-performance computing for rapid application to region-scale (e.g., CONUS) 2-meter resolution imagery datasets. Our approach is tailored to sensors that collect data at two-meter resolution with high return times for frequent updates. We mapped 591 WorldView satellite images for Florida, North Carolina, and Alaska and validated the maps against LiDAR-derived bathymetry data. Results show median RMSE of 1.75, 1.59, and 2.67 meters, respectively. By combining the strengths of Oak Ridge National Laboratory in high-performance computing and remote-sensing science with the water-column modeling expertise of Scripps Institution of Oceanography we advance the state of bathymetric mapping capability.

1. INTRODUCTION

Traditional approaches to mapping bathymetry rely on ship soundings or light detection and ranging (LiDAR) measurements from aerial vehicles that are costly, labor-intensive, spatially limited, and time-consuming. As a result, approximately 70-80% of the global coastal zone lacks accurate bathymetry maps, let alone those of high spatio-temporal resolution. Satellite-derived bathymetry (SDB) algorithms exist but are either trained for local applications only or require ancillary data such as benthic substrate maps or in-situ water quality data coinciding with satellite retrievals to produce accurate results. Further, the local satellite-based models tend to inaccurately estimate water-column light attenuation in shallow coastal scenes where turbidity varies throughout the image, resulting in poor performance unless water clarity is known and uniform across a scene.

Estimating water column optical properties accurately has long been a barrier to coastal monitoring in the field of optical remote sensing. It is particularly challenging in areas where the benthic substrate (e.g. coral, sand, hard bottom, seagrass) is diverse and unknown (i.e. unmapped), and because water-column optical properties can vary significantly over relatively small scales (meters to hundreds of meters) in coastal environments. Our approach to resolve this issue and automate the mapping of bathymetry from optical satellite imagery is to develop algorithms that estimate water column inherent optical properties (IOPs) from commercial high-resolution (i.e., 2-meter) WorldView imagery on a pixel-by-pixel basis and include these effects in a new bathymetry model formulation that uses the satellite-derived band ratio of ocean reflectance as input to derive the bottom depth. This band-ratio formulation itself is an improvement over previous formulations of band ratio used in bathymetry models (Stumpf et al., 2003). The advent of satellites designed specifically with sensor characteristics to facilitate the retrievals of light-attenuating water components like suspended particulate matter (SPM) has paved the way for algorithms that can transfer coarse-resolution open-ocean models to high-resolution coastal applications. Advancing the model behind water column attenuation estimation is one of the key elements of this research.

2. MATERIALS AND METHODS

2.1 Study Areas

The sites selected for this study include south Florida, the North Carolina coast, and Cook Inlet, Alaska (Figure 1). The former includes the Florida Keys, Florida Bay, and part of the southeastern Florida coast. The region is characterized by a mix of bottom types (e.g., sand, coral, seagrass) with relatively turbid water in Florida Bay from riverine input, and relatively clear water south of the Keys and along the coast. The North Carolina study area included the Albermarle-Pamlico Sound, which is a shallow turbid estuary, as well as the Atlantic side of the Outer Banks. Cook Inlet is a relatively deep water body that is challenging for SDB because of its high latitude and subsequently low incoming solar radiation.

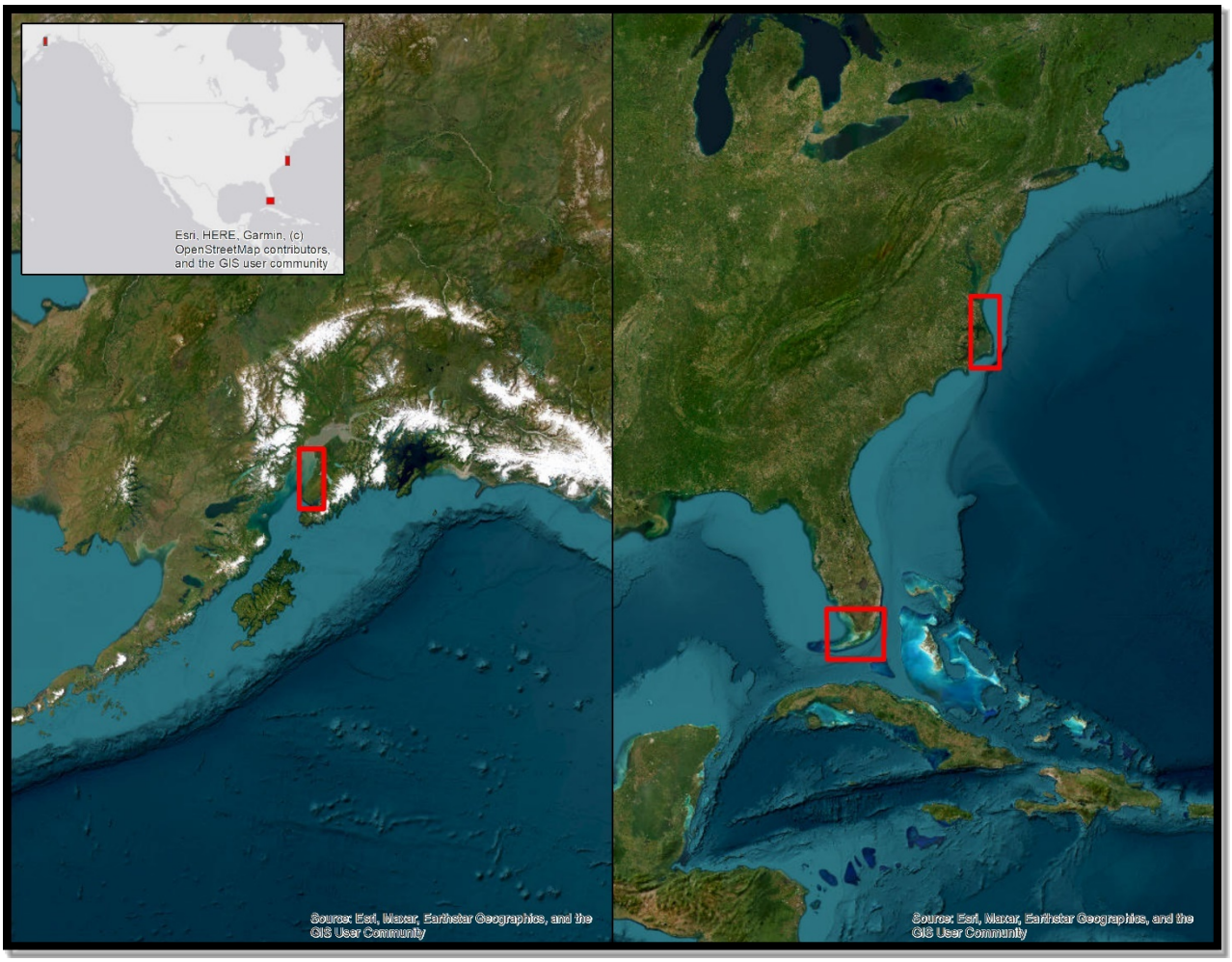

Figure 1. Study areas mapped for this project: Cook Inlet, Alaska; south Florida; and coastal North Carolina.

2.2 Satellite Data and Preprocessing

Level-1B WorldView images were acquired through the NextView License for each study site. A total of 589 images were acquired: 171 for Florida, 233 for North Carolina, and 185 for Alaska. WorldView imagery has high radiometric resolution, near-daily repeat time, and has been used successfully to map

bathymetry in small-scale study areas (Kerr and Purkis, 2018). Of the 8 multispectral bands of WorldView-2 and WorldView-3, there are 6 bands required by the overall water column algorithm, referred to as the Coastal Blue (CB), Blue (B), Green (G), Yellow (Y), Red (R), and Red Edge (RE) bands. The spectral characteristics of these bands vary slightly between the two WorldView sensors; the center wavelengths and spectral ranges for these respective bands are 427 ± 31, 478 ± 37, 546 ± 41, 608 ± 24, 659 ± 35, and 724 ± 25 nm for WorldView-2, and 426 ± 29, 481 ± 36, 547 ± 40, 605 ± 25, 661 ± 35, and 724 ± 26 nm for WorldView-3.

All images were radiometrically calibrated and then atmospherically corrected using Py6S, which is a Python wrapper for the robust Second Simulation of the Satellite Signal in the Solar Spectrum (6S) model. Atmospheric correction is a vital element in aquatic remote sensing given that the water-leaving signal may constitute less than 10% of satellite-detected solar radiation, thereby requiring accurate estimation and correction of the atmospheric contribution to ensure accurate water-leaving retrievals. The 6S algorithm is one of the most robust radiative transfer models available for atmospheric correction yet is also computationally efficient for rapid processing. We implemented the 6S model to atmospherically correct WorldView spectral bands by accounting for viewing geometry (i.e., sun/sensor azimuth and zenith angles), Earth-Sun distance, sensor and target altitude, dominant aerosol types, water vapor, and ozone. Aerosol optical thickness (AOT) was determined by first identifying optically deep water (ODW) pixels in the image (McCarthy et al., 2022), then iteratively running the Py6S model across a range of AOT values (i.e. 0.01 to 0.6 at 0.05 intervals), calculating spectral reflectance for the ODW pixels in the near-infrared (i.e., WorldView band 7), and selecting the AOT value that produced the lowest non-negative result under the assumption that the near-infrared reflectance over ODW should be approximately zero. AOT is a critical component of coastal atmospheric attenuation but is difficult to assess and therefore often treated as a constant. Our method allows us to efficiently estimate AOT for a more accurate correction.

The resulting surface remote-sensing reflectance (Rrs) values for each pixel were then automatically assessed for sunglint presence. Sunglint, also known as specular reflection, occurs when sunlight reflects off a water surface at such an angle to result in near saturation to saturation of the satellite sensor, thereby confounding the use of glinted pixels for bathymetric estimation. We developed automated algorithms to predict glint likelihood, identify individual glinted pixels, and correct them to be usable for bathymetry mapping (McCarthy et al. 2022). Predicting the likelihood of glint in an image has historically been done using a probability density function based on sun-sensor geometry (Cox and Munk, 1954). We developed a similar function to rapidly estimate glint likelihood. High likelihood would then trigger a search of every pixel for a glint-specific spectral profile (McCarthy et al., 2020). Glinted pixels are then corrected using the robust linear-regression method of Hedley et al. (2005) that we revised to automate the identification of glinted versus glint-free pixels, thereby improving computational efficiency over previous manual methods.

2.3 Physics-based Bathymetry Model

The physics-based bathymetry model developed as part of this project consists of two main components, a first component that estimates the inherent optical properties (IOPs) of the water column, and a coupled second component which addresses the retrieval of bottom depth using a Look-Up Table (LUT) approach. A schematic illustrating the fundamental steps of the physics-based bathymetry model for deriving bottom depth from WorldView imagery is depicted in Figure 2. For a given pixel, the model utilizes the atmospherically-corrected spectral remote sensing reflectance, $R_{rs}(\lambda)$, derived from WorldView satellite imagery to estimate the concentration of suspended particulate matter (SPM) in the water column (Step 1). SPM serves as a proxy for the water column IOPs specific to particulate constituents. Step 2 involves the use of particulate IOP algorithms tailored for WorldView Coastal Blue (CB), Blue (B), and Green (G)

bands, leveraging the strong relationships between SPM and spectral particulate IOPs (i.e., particulate absorption and backscattering coefficients). Step 3 addresses the contribution to absorption by chromophoric dissolved organic matter (CDOM) in the water column by utilizing reflectance-based CDOM algorithms developed for WorldView Blue and Green bands. The total IOPs are then determined through summation including the contributions of pure seawater. The spectral absorption coefficient of pure seawater, $a_w(\lambda)$, is based upon values recommended in the IOCCG Protocol Series (2018) while the spectral backscattering coefficient, $b_{bw}(\lambda)$, is calculated assuming specific water temperature and salinity conditions (Zhang et al., 2009).

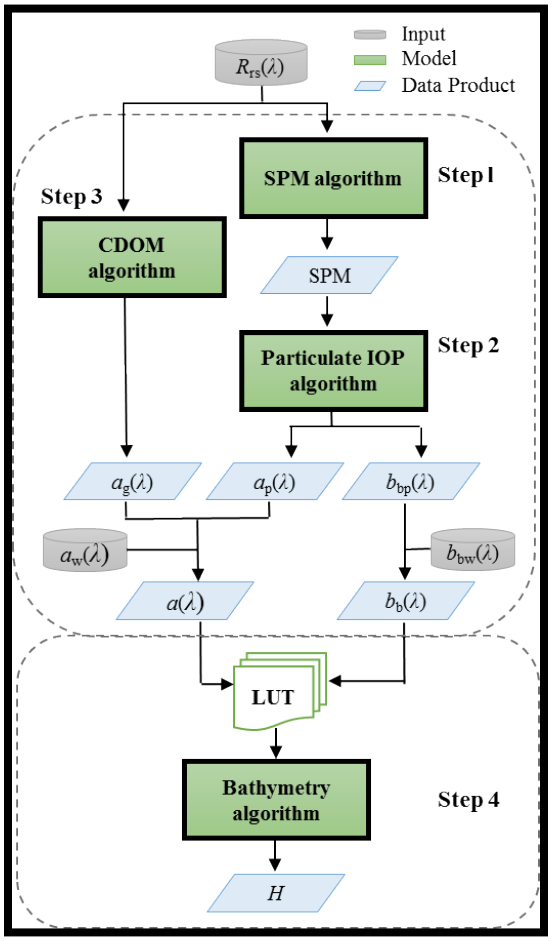

Figure 2. Flowchart depicting basic steps in the operation of the physics-based bathymetry model.

In the bottom depth retrieval component of the model (Step 4 in Fig. 2), bulk IOPs of seawater obtained from the water column component (Steps 1–3) are utilized in an optimization scheme to search within precomputed LUTs for the most representative IOP scenario. Once the best match is determined for a given pixel, the associated blue-to-green-band-ratio-bathymetry algorithm is applied to compute the bottom depth H from the satellite-derived $R_{rs}(\lambda)$ obtained from WorldView.

2.3.1 Development of water column component of the physics-based bathymetry model

The water column component focuses on estimating two key IOPs of seawater; the total absorption coefficient, $a(\lambda)$, and the backscattering coefficient, $b_b(\lambda)$, both of which significantly influence light propagation within the water column and contribute to ocean remote-sensing reflectance. The total IOPs

are treated as the sum of partial contributions from optically-significant water constituents. For instance, the total absorption coefficient comprises contributions from pure seawater, particles, and CDOM, i.e., $a(\lambda) = a_w(\lambda) + a_p(\lambda) + a_g(\lambda)$. Similarly, the total backscattering coefficient includes contributions from pure seawater and particles, i.e., $b_b(\lambda) = b_{bw}(\lambda) + b_{bp}(\lambda)$. The concentration of suspended particulate matter is typically the first-order determinant of light scattering and absorption properties in natural waters, and thus the water-column model first estimates SPM from WorldView-derived $R_{rs}(\lambda)$, which is subsequently used to calculate the IOPs associated with particulate matter. The absorption of CDOM is estimated in a separate step.

Three distinct sets of field data were used to formulate algorithms for the different steps of the water column component of the physics-based bathymetry model: 1) coexisting measurements of SPM and $R_{rs}(\lambda)$ for the development of the SPM algorithm in Step 1, 2) concurrent measurements of SPM, $a_p(\lambda)$, and $b_{bp}(\lambda)$ for development of the particulate IOP algorithms in Step 2, and 3) coexisting measurement of $a_g(\lambda)$ and $R_{rs}(\lambda)$ for development of the model to estimate the spectral absorption coefficient of CDOM in Step 3. Field datasets meeting the criteria of simultaneous measurements of SPM, IOPs of constituents, and radiometric quantities with high spectral resolution are generally scarce. Over recent decades, the Scripps Institution of Oceanography (SIO) team along with collaborators has undertaken numerous field campaigns to gather such data across a range of open ocean and coastal settings, from tropical to high-latitude regions. Valuable datasets for this endeavor were gathered and collated from approximately 200 stations in the Atlantic, Pacific, and Southern Oceans (Reynolds et al., 2001; Stramski et al., 2008), along with around 140 stations from Arctic expeditions (Reynolds et al., 2016; Reynolds and Stramski, 2019).

For the development of algorithms related to SPM for WorldView-2 and WorldView-3 satellites, a meticulously quality-controlled field dataset comprising 123 concurrent SPM and $R_{rs}(\lambda)$ measurements with high spectral resolution was curated from seven cruises spanning the Arctic, Atlantic, and Pacific oceanic basins. This dataset exhibits a wide dynamic range of SPM concentrations, from approximately 40 mg m^{-3} to 20,000 mg m^{-3}, and R_{rs} spectra representing waters ranging from ultraoligotrophic clear conditions to turbid coastal waters dominated by minerals. Due to differences in spectral response functions between field instruments and WorldView sensors, the field measurements of $R_{rs}(\lambda)$ were adjusted by spectral weighting using the spectral response functions of WorldView sensors, thereby obtaining WorldView band-specific spectrally weighted average R_{rs}. Various combinations of data subsets and mathematical models were explored to derive an optimal algorithm for estimating SPM concentration using the Red (R) and Red Edge (RE) bands of WorldView sensors. The use of these bands is advantageous because it allows determination of SPM in shallow waters without the effect of bottom reflectance on water-leaving light. To optimize overall performance across a range of SPM, a hybrid SPM algorithm was formulated by integrating the Red-band and Red Edge-band algorithms using a weighting approach and a switch based on the RE reflectance threshold.

A dataset comprising 355 simultaneous field measurements of SPM and $a_p(\lambda)$ was assembled to develop algorithms pertaining to spectral particulate absorption coefficients tailored for WorldView-2 and WorldView-3 satellites. Following an assessment of mathematical models using various statistical metrics, a power function was chosen as the final algorithm formulation to predict $a_p(\lambda)$. from SPM for the Coastal Blue (CB), Blue (B), and Green (G) bands of WorldView-2 and WorldView-3. Likewise, distinct quadratic algorithms were developed to estimate particulate backscattering coefficient b_{bp} for the CB, B, and G bands of WorldView sensors from SPM, utilizing a dataset comprising 311 co-existing field measurements of SPM and $b_{bp}(\lambda)$.

The chromophoric dissolved organic matter (CDOM) is another major constituent of the water column that attenuates light strongly via absorption and affects the contribution of the water column to the water-leaving radiance. To account for the role of CDOM contribution to ocean reflectance, 3-band multiple linear regression algorithms were developed for estimating the absorption coefficient of CDOM at CB, B,

and G bands of WorldView sensors using 142 concurrent field measurements of $a_g(\lambda)$ and $R_{rs}(\lambda)$ collected in optically deep waters.

2.3.2 Development of bottom depth retrieval component of the physics-based bathymetry model

The primary objective of this component was to construct Look-Up Tables (LUTs) containing bathymetry model coefficients tailored to predefined solar zenith angles (i.e., 0°, 30°, and 60°), bottom types (i.e., dark, bright, and mixed bottom), and a specified set of spectral inherent optical properties of the water column (specifically, absorption coefficient $a(\lambda)$ and backscattering coefficient $b_b(\lambda)$) for determining bottom depth from the blue-to-green band ratio of remote-sensing reflectance. The LUTs were generated from the results of forward modeling simulations of optically-shallow subsurface remote sensing reflectance $r_{rsOS}(\lambda)$ using a semi-analytical model (Lee et al., 1998; 1999). For a nadir-viewing observation angle and an arbitrary light wavelength λ, this model provides an approximate expression for $r_{rs}(\lambda)$ as a sum of contributions from the water column $r_{rs}{}^{C}$ and from the bottom, $r_{rs}{}^{B}$:

$$r_{rsOS}(\lambda, H) = r^{rsC}(\lambda) + r^{rsB}(\lambda) = r_{rsOD}(\lambda) \times \left[1 - e^{-\left\{\left[\left(\frac{1}{\cos(\theta_w)}\right) + D\upsilon^{C}(\lambda)\right] \times \kappa(\lambda) \times H\right\}}\right] + \left(\frac{\rho_{bottom}(\lambda)}{\pi}\right) \times \left[e^{-\left\{\left[\left(\frac{1}{\cos(\theta_w)}\right) + D\upsilon^{B}(\lambda)\right] \times \kappa(\lambda) \times H\right\}}\right] \quad (1)$$

where θ_w is the subsurface solar zenith angle calculated using Snell's refraction law for air-water interface, r_{rsOD} is the subsurface reflectance for optically deep water, κ is the light attenuation coefficient within the water column ($\approx a + b_b$), and $D\upsilon^{C}$and $D\upsilon^{B}$ are the optical path-elongation factors for scattered photons from water column and bottom, respectively. Importantly, in this model r_{rsOD}, κ, $D\upsilon^{C}$ and $D\upsilon^{B}$ are all quantified through approximate relationships dependent only on two IOPs of seawater, namely the total absorption coefficient, a, and the total backscattering coefficient, b_b. Thus, this model provides a means to calculate $r_{rsOS}(\lambda)$ for any given solar angle θ_S, the seawater absorption and backscattering coefficients $a(\lambda)$ and $b_b(\lambda)$, the bottom reflectance $\rho_b(\lambda)$, and the bottom depth H.

Field datasets alone cannot provide the full range, resolution, and combinations of input data (i.e., $r_{rsOD}(\lambda)$, $\rho_b(\lambda)$, $a(\lambda)$ and $b_b(\lambda)$) needed for such simulations and thus synthetic datasets are commonly used for this purpose. As part of a prior NASA Plankton, Aerosol, Cloud, ocean Ecosystem (PACE) project, the SIO team collaborated with researchers in France to generate a new synthetic dataset of ocean optical properties created through radiative transfer simulations conducted with 3320 combinations of input IOPs (Loisel et al., 2023). The IOPs in these simulations cover a broad spectral range (300–800 nm) with high (5 nm) spectral resolution. Crucially, the probability distributions of these synthetic IOP scenarios have been designed to match the actual variability patterns observed in seawater absorption and backscattering coefficients across the global ocean. Multiple radiative transfer simulations were executed for each IOP combination assuming an optically-deep ocean and incorporating varying scenarios of boundary conditions (e.g., different solar zenith angles) and the presence of inelastic radiative processes (Raman scattering and fluorescence), resulting in a database of approximately 30,000 total simulations. For each IOP scenario, these radiative transfer simulations provided the remote sensing reflectance term for optically-deep water, $r_{rsOS}(\lambda)$, which is also required in Eq. (1). The synthetic database represents a unique resource and was the source of coexisting $r_{rsOD}(\lambda)$, $a(\lambda)$ and $b_b(\lambda)$ used to conduct the forward model simulations with the semi-analytical model (Eq. 1) to obtain ultimate algorithm formulas for estimating the bottom depth H from WorldView-derived reflectance measurements.

Reflectance spectra corresponding to three generic bottom types (dark, bright, and mixed bottom), $\rho_b(\lambda)$, were obtained from the PANGAEA data repository (Roelfsema and Phinn, 2017). The initial use of these

three generic bottom reflectance spectra is adequate for the demonstration of the development and application of bathymetry algorithm in this project. However, the scheme of the forward modeling approach allows to readily expand the bathymetry algorithms by expanding the LUTs using any bottom reflectance spectrum.

For each of the 3320 combinations of water column IOPs, including subsurface remote-sensing reflectance for optically deep water $r_{rsOD}(\lambda)$, bottom type, solar zenith angle, and nadir sensor viewing angle, the forward model (Eq. 1) was executed across variable bottom depths ranging from 0.1 m to 50 m at intervals of 0.1 m (resulting in 500 depths). This process yields depth-dependent subsurface remote-sensing reflectance $r_{rsOS}(\lambda)$ for optically shallow waters, incorporating contributions from both the water column and bottom substrate. After determining the spectrally-weighted average subsurface remote-sensing reflectance for the blue $r_{rsOSw}(B)$ and green $r_{rsOSw}(G)$ bands of WorldView sensors using spectral response functions, a relationship between 500 bottom depths and 500 WorldView-specific blue-to-green reflectance band ratios was examined. This procedure was repeated for all 3320 IOP scenarios to derive 3320 relationships between bottom depth (*H*) and blue-to-green (B-G) reflectance ratio, each of which allows to define a specific algorithm for calculating bottom depth from blue-to-green reflectance ratio for a given IOP scenario, solar zenith angle, and bottom type. Overall, for a given solar zenith angle and bottom type, 1,660,000 (3320 IOP scenarios x 500 bottom depths) spectra of $r_{rsOS}(\lambda)$, each with a 1-nm resolution in the range 350-750 nm, were computed from Eq. (1). As these computations were made for 3 solar zenith angles and also for 3 bottom types, the overall process of simulations with Eq. (1) generated 14,940,000 spectra of $r_{rsOS}(\lambda)$ specific to each of the two WorldView sensors.

To appropriately constrain the applicability of the bathymetry model and ensure reasonable bottom depth estimates across a range of water types from clear to turbid waters, a maximum bottom depth threshold was determined for each of the 3320 *H* vs. B-G ratio relationships. This threshold is used as a criterion for the range of applicability of any given bathymetry algorithm associated with specific IOPs of water column.

Subsequently, a cubic polynomial function was fitted to the data of bottom depth vs. blue-to-green reflectance band-ratio within the range from 0.1 m to the bottom depth threshold for each of the 3320 IOP scenario-specific relationships between *H* and B-G band ratio. These third-order polynomial functions represent the bathymetry algorithms corresponding to the 3320 different IOP scenarios:

$$H = \beta_0 + \beta_1 \left(\frac{r_{rsOSw}(B)}{r_{rsOSw}(G)}\right) + \beta_2 \left(\frac{r_{rsOSw}(B)}{r_{rsOSw}(G)}\right)^2 + \beta_3 \left(\frac{r_{rsOSw}(B)}{r_{rsOSw}(G)}\right)^3 \quad (2)$$

A single Look-Up Table (LUT) was created specifically for each bottom type, solar zenith angle, and sensor viewing angle. Each specific LUT contains the best-fit coefficients (i.e., β_0, β_1, β_2, and β_3) of the 3320 bathymetry algorithms associated with a given set of spectral IOPs of seawater, along with additional information on corresponding IOPs, IOP ratios (i.e., $b_b/(a+ b_b)$), and optically deep-water reflectances at WorldView spectral bands. Additionally, the LUT includes IOP-related water class, bottom depth threshold, and SPM derived from deep-water reflectances for each of the 3320 bathymetry models. For each bottom type, a set of three LUTs corresponding to solar zenith angles of 0°, 30°, and 60° was developed, resulting in a total of 9 LUTs corresponding to combinations of three bottom types (bright, dark, and mixed bottom) and three solar zenith angles for each WorldView sensor.

2.3.3 Implementation of the physics-based bathymetry model to WorldView imagery

The LUTs generated by the forward modeling simulations of reflectance were used for inverting remotely sensed reflectances to extract environmental information on SPM, water-column inherent optical

properties, and bathymetry. The LUT methodology works by comparing the satellite-derived IOP ratios for the C, B, and G bands ($a(\lambda)/(a(\lambda) + b_b(\lambda))$ for a particular image pixel with each IOP ratio in the appropriately-chosen LUT, and the closest match is identified by finding a minimum of the sum of squared differences between the satellite-derived and LUT-database ratios. The bathymetry model coefficients are then extracted from the LUT and applied as in Equation 2 to map depth for that pixel. Once all pixels are mapped for an image, values less than 0 (i.e., erroneous) and greater than 50 (i.e., beyond the scope of this work) are set to 0, and masks for land and cloud are applied to set those pixels to 0. Maps are output as GeoTIFFs with georeferencing, and mosaicked for each study area in ArcMap. The initial version of this algorithm uses the mixed bottom type as the default, but the user may manually set the desired bottom type for LUT usage for a study area if the dominant bottom type is known to be dark or bright. For solar zenith angle, the appropriate LUT is automatically selected by extracting the solar zenith angle from the metadata file for each image and choosing the LUT that most closely aligns with it.

2.4 Validation

LiDAR-based digital topobathymetry models (DTMs) were used to validate the satellite-derived bathymetry maps for each location. DTMs were downloaded from the NOAA Digital Coast data portal (coast.noaa.gov/dataviewer). For each study area DTM, random points were generated in ArcMap for the maximum number of points that would fit within the extent of the DTM and maintain separation of at least 10 meters to avoid spatial autocorrelation. Any land points were eliminated, as well as any areas of the DTMs that showed scattered returns that might indicate poor LiDAR measurements (McCarthy et al., 2022). Bathymetry values were extracted to each point for the DTMs and WorldView maps, and any NaN, land or cloud values were eliminated from final consideration.

Tide correction was not applied to the DTMs, and therefore tide correction could not be applied for validation of the study area maps, but tide correction is typically not performed for SDB in the literature, and the tidal amplitude of the FL and NC study sites is minimal (approximately 0.39m and 0.27m, respectively). Alaska's tidal amplitude, however, is substantial (i.e., approximately 4.8m), and validation of our product was necessary. Unfortunately, DTMs within the study area did not include tide correction, but we were able to acquire timestamped LiDAR validation data for one site nearby the study area (i.e., outside of the target region of interest but within Cook Inlet) with which to validate the Alaska product. One WorldView image was acquired and processed to cover the additional study site and is used to represent the accuracy of the Alaska study area. Tidal height at time of acquisition was determined for the LiDAR data and image based on the Coal Point tide gauge (station 9455558, tidesandcurrents.noaa.gov) and subtracted from the bathymetry retrievals to determine tide-corrected bathymetry.

3. RESULTS

3.1 Bathymetry Results

Maps of the study areas are shown in Figures 3-5 below. All maps produced for this report were processed with the Mixed bottom-type WorldView-2 LUTs, and the solar zenith angle was automatically selected from the metadata as follows: angles less than 15 degrees used the 0-degree LUT; angles between 15 and 45 degrees used the 30-degree LUT; and angles greater than 45 used the 60-degree LUT. These selections assume that the Mixed LUT best represents the influence of bottom spectra in an area with a variety of bottom types (e.g. mix of sand, seagrass, coral, rubble, etc.). However, if the user knows the area's benthic cover is dominated by bright or dark substrate, we recommend selecting those for processing. Additionally, we assume that three solar zenith angle ranges sufficiently represent the sensitivity of the algorithm to solar radiation influence. The WorldView-3 LUTs were not available at the

time of processing, so all WorldView-3 images were run with the LUTs built for WorldView-2. Rerunning with the LUTs specific to each sensor will likely further improve results.

Processing all 589 images required advanced computational solutions for efficiency. For reference, using a 4-core CPU with 30GB RAM, looping through each of the roughly 64 million pixels in an image would require approximately 14 days to complete bathymetry mapping per image. The majority of the algorithm's processing time is dedicated to the final bathymetry mapping step because the pixel-by-pixel approach adopted here requires that each pixel be treated individually. That is, each pixel is mapped by selecting the optimal LUT solution based on the values representing the optical properties specific to that pixel (i.e., $a(\lambda)$ and $b_b(\lambda)$) and therefore could not be mapped *en masse* using array math operations. Our approach completed mapping in approximately 3 hours per image without leveraging high-performance computing clusters, GPU acceleration, or parallelization. All of these optimization approaches are valid for running the algorithm, and delivery to the sponsor conservatively assumed that none of these methods would be available so that the algorithm could run with minimal resources for efficiency. Hence, additional speed optimization is possible with further development. The delivered solution only requires a single CPU core and 30GB of RAM, which are typical of today's standard laptops.

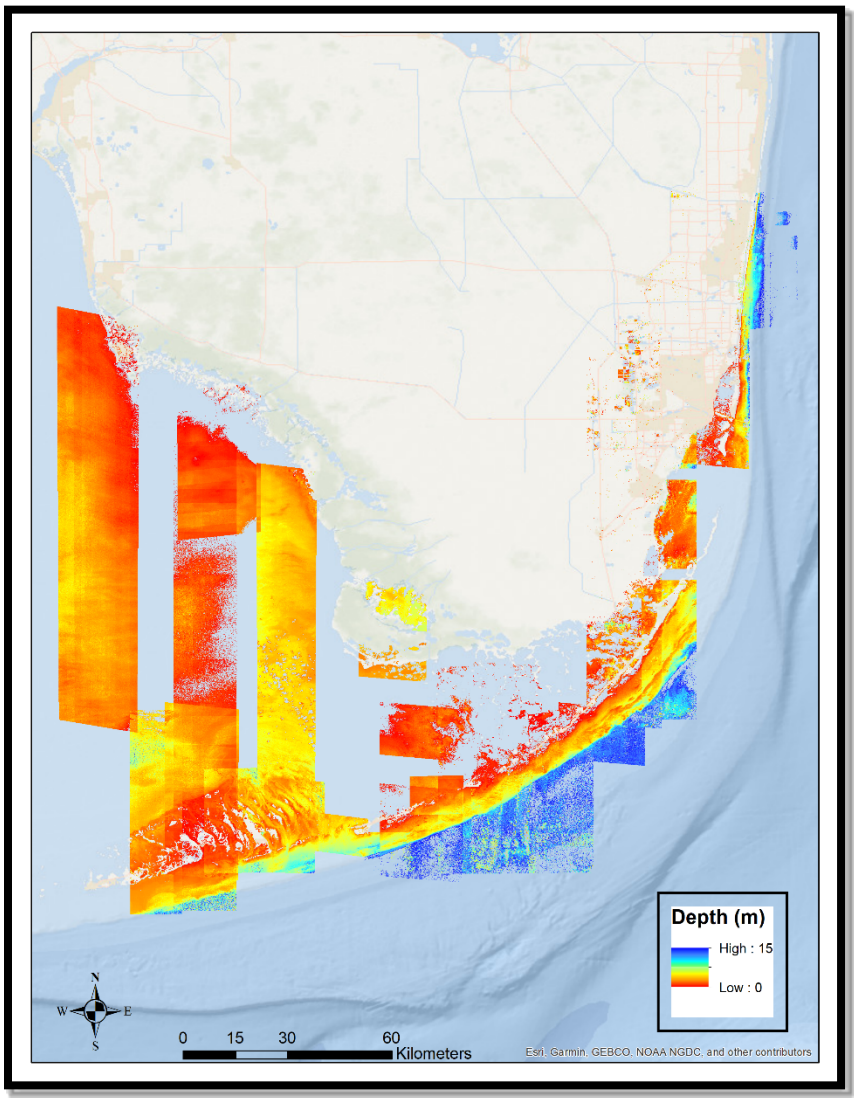

Figure 3. Bathymetry map of south Florida study area.

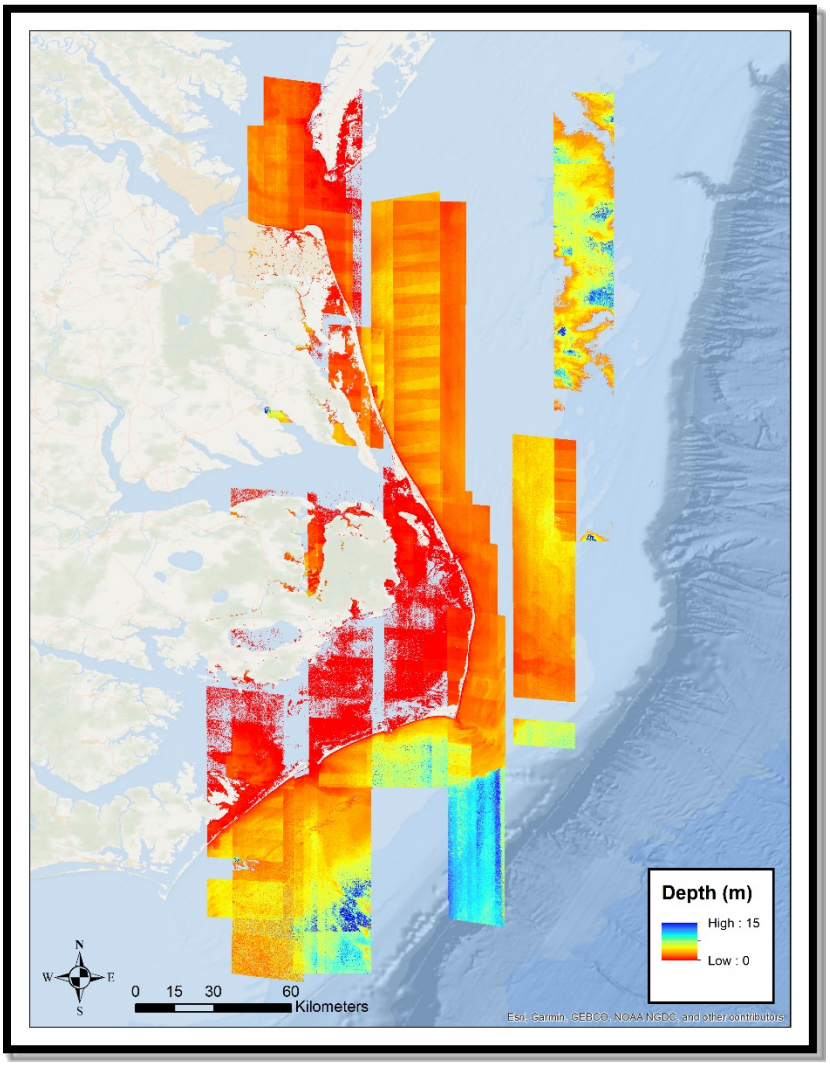

Figure 4. Bathymetry map of North Carolina study area.

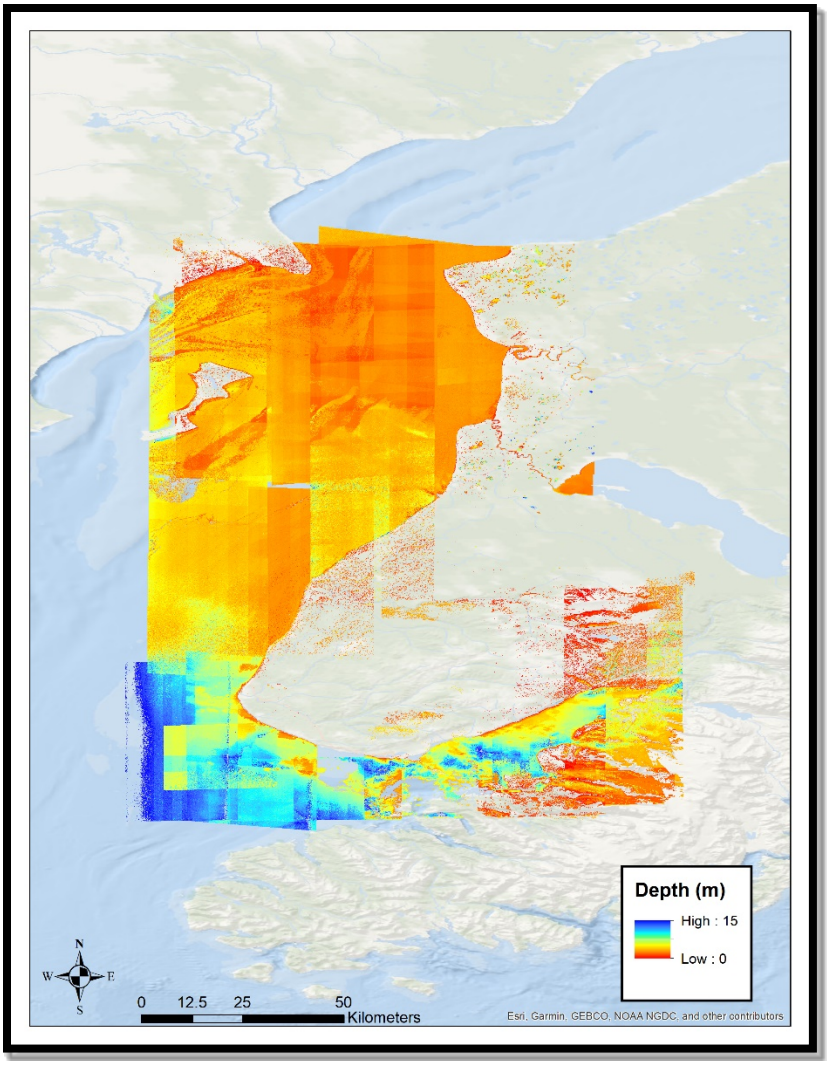

Figure 5. Bathymetry of Cook Inlet, Alaska study area.

3.2 Bathymetry Validation

Validation was conducted on an image-by-image basis rather than using the mosaicked maps, which would introduce bias where images overlap. Root-mean-squared-error (RMSE) was calculated for each image map, and the mean, median, minimum, and maximum are reported for all validated images per study area in Tables 1-4. Of the 591 images mapped, 50 images overlapped with validation data for Florida, and 77 images overlapped with validation data for North Carolina. For Alaska, the RMSE of the single tide-corrected validation image is reported.

Spot checks of mapped results show that some images contain artifacts that resulted in poor bathymetry retrievals (e.g., striping, haze). Table 1 displays the results for all validated images without removing poor images from validation consideration so as to wholistically represent the performance of the algorithm when applied to a large sample of WorldView imagery.

Table 1. Validation results for bathymetry maps by study area.

	Florida (n=50)	**North Carolina** (n=77)	**Alaska** (n=1)
Median RMSE (m)	1.75	1.59	2.67
Mean RMSE (m)	2.02	1.99	
Min RMSE (m)	0.60	0.23	
Max RMSE (m)	4.58	5.53	

Evaluation of images during quality control found four primary causes of poor accuracy (i.e. > 2.5m RMSE): cloud and cloud shadow, haze, striping, and poor sampling. The latter refers to images for which few validation points overlapped (e.g. < 10 points), or points were clustered in a small section of the image precluding a representative evaluation. When these images were removed, validation was recalculated and the results are shown in Table 2. Table 3 displays the results broken out by depth bin.

Table 2. Validation results for bathymetry maps by study area after quality control.

	Florida (n=43)	**North Carolina** (n=56)	**Alaska** (n=1)
Median RMSE (m)	1.70	1.33	2.67
Mean RMSE (m)	1.79	1.36	
Min RMSE (m)	0.60	0.23	
Max RMSE (m)	3.72	2.49	

Table 3. Florida validation results by bin depth after quality control.

Depth	Median RMSE (m)	Mean RMSE (m)	Min RMSE (m)	Max RMSE (m)
0-15	1.70	1.79	0.60	3.72
0-2	1.33	1.38	0.60	2.84
2-4	1.66	1.64	0.50	3.63
4-6	2.05	2.21	0.69	4.56
6-8	2.86	2.95	1.00	5.64
8-10	3.06	3.61	1.33	8.63
10-12	3.74	4.58	1.49	9.90
12-15	3.96	4.53	2.16	9.49

Table 4. North Carolina validation results by bin depth after quality control.

Depth	Median RMSE (m)	Mean RMSE (m)	Min RMSE (m)	Max RMSE (m)
0-15	1.33	1.36	0.23	2.49
0-2	1.04	1.12	0.23	2.87
2-4	1.93	1.85	0.92	2.64
4-6	4.09	3.64	1.44	4.83
6-8	6.29	6.29	6.12	6.45
8-10	N/A	N/A	N/A	N/A
10-12	N/A	N/A	N/A	N/A
12-15	N/A	N/A	N/A	N/A

Table 4. Alaska validation results by bin depth after quality control.

Depth	RMSE (m)
0-15	2.67
0-2	3.48
2-4	3.21
4-6	2.04
6-8	2.38
8-10	3.02
10-12	3.99
12-15	5.25

4. CONCLUSIONS

This study developed and applied a novel automated model for atmospherically correcting, estimating water column inherent optical properties (IOPs) and mapping coastal bathymetry from satellite imagery at 2-meter resolution. The three study areas mapped represent a challenging diversity of IOPs and bottom types that demonstrate the flexible nature of the algorithm to map virtually any coastal water body. Our target accuracy was under 2-meters RMSE, which we met for Florida and North Carolina, but not for Alaska. One explanation for Alaska is that the tide gauge contained preliminary data, not verified data, which indicates it was predicted but not confirmed. Given the 4.8-meter tidal amplitude at the location, a slight difference in verified versus predicted tide level could have substantial impact on the validation. There were, as expected, image subsets that could not be mapped accurately as they contained water that was too optically deep, meaning the depth was beyond 15-meter limit targeted for this study or the water was too turbid for the minimum water-leaving retrieval required to estimate depth.

Processing was completed in an average time of 3 hours per image on a 4-core CPU with 30GB of RAM. There is ample room for speed improvement with optimization methods depending on what resources the sponsor may want to leverage. In addition to processing speed, future work could focus on expanding the LUTs to cover a more extensive variety of conditions (e.g., specific benthic habitat types such as coral and seagrass rather than generic types, accounting for solar zenith angle with higher resolution), running sensitivity analyses for the various components, and automating the correction for tidal amplitude, among other potential avenues for research. Transferring this protocol to other sensors would require modification of the atmospheric correction algorithm to include the sensors' specifications (e.g., calibration factors, effective bandwidths, center wavelengths), reprocessing the IOP algorithms for the spectral response functions of the sensor's bands, and subsequent generation of new look-up-tables. However, for the results shown here, only WorldView-2 LUTs were used to process both WorldView-2 and WorldView-3 images (i.e., WorldView-3 LUTs were not yet available). Results show consistent performance regardless of sensor, so it is plausible that simply running the algorithms as developed here on sensors with similar bands could produce reasonable results, if not as accurate as those produced here.

5. REFERENCES

Cox, C., Munk, W., 1954. Measurement of the Roughness of the Sea Surface from Photographs of the Sun's Glitter. J. Opt. Soc. Am. 44, 838. https://doi.org/10.1364/JOSA.44.000838

Hedley, J.D., Harborne, A.R., Mumby, P.J., 2005. Technical note: Simple and robust removal of sun glint for mapping shallow-water benthos. International Journal of Remote Sensing 26, 2107–2112. https://doi.org/10.1080/01431160500034086

IOCCG. 2018. Inherent Optical Property Measurements and Protocols: Absorption Coefficient, in: IOCCG Ocean Optics and Biogeochemistry Protocols for Satellite Ocean Colour Sensor Validation, edited by: Neeley, A. R. and Mannino, A., vol. 1.0, 78 pp., IOCCG, Dartmouth, NS, Canada, https://doi.org/10.25607/OBP-119.

Kerr, J.M., Purkis, S., 2018. An algorithm for optically-deriving water depth from multispectral imagery in coral reef landscapes in the absence of ground-truth data. Remote Sensing of Environment 210, 307–324. https://doi.org/10.1016/j.rse.2018.03.024

Lee, Z., K. L. Carder, C. D. Mobley, R. G. Steward, and J. S. Patch. 1998. Hyperspectral remote sensing for shallow waters. 1. A semianalytical model. Appl. Opt., 37, 6329–6338.

Lee, Z., K. L. Carder, C. D. Mobley, R. G. Steward, and J. S. Patch. 1999. Hyperspectral remote sensing for shallow waters: 2. Deriving bottom depths and water properties by optimization. Appl. Opt., 38, 3831–3843.

Loisel, H., D. S. F. Jorge, R. A. Reynolds, and D. Stramski. 2023. A synthetic optical database generated by radiative transfer simulations in support of studies in ocean optics and optical remote sensing of the global ocean, Earth Syst. Sci. Data, 15, 3711–3731, https://doi.org/10.5194/essd-15-3711-2023.

McCarthy, M.J., 2018. Enabling efficient, large-scale high-spatial resolution wetland mapping using satellites. Remote Sensing of Environment 13.

McCarthy, M.J., Jessen, B., Barry, M.J., Figueroa, M., McIntosh, J., Murray, T., Schmid, J., Muller-Karger, F.E., 2020. Automated High-Resolution Time Series Mapping of Mangrove Forests Damaged by Hurricane Irma in Southwest Florida. Remote Sensing 12, 1740. https://doi.org/10.3390/rs12111740

McCarthy, M.J., Otis, D.B., Hughes, D., and F.E. Muller-Karger. Automated high-resolution satellite-derived coastal bathymetry mapping. Int. J. Appl. Earth Obs. Geoinformation, vol. 107, p. 102693, Mar. 2022, doi: 10.1016/j.jag.2022.102693.

Reynolds, R. A., and D. Stramski. 2019. Optical characterization of marine phytoplankton assemblages within surface waters of the western Arctic Ocean. Limnol. Oceanogr., 64, 2478–2496. doi: 10.1002/lno.11199.

Reynolds, R. A., D. Stramski, and B. G. Mitchell. 2001. A chlorophyll-dependent semianalytical reflectance model derived from field measurements of absorption and backscattering coefficients within the Southern Ocean. J. Geophys. Res., 106(C4), 7125–7138.

Reynolds, R. A., D. Stramski, and G. Neukermans. 2016. Optical backscattering by particles in Arctic seawater and relationships to particle mass concentration, size distribution, and bulk composition. Limnol. Oceanogr., 61, 1869–1890.

Roelfsema, C., and S. R. Phinn. 2017. Spectral reflectance library of healthy and bleached corals in the Keppel Islands, Great Barrier Reef. PANGAEA, https://doi.org/10.1594/PANGAEA.872507

Stramski, D., R. A. Reynolds, M. Babin, S. Kaczmarek, M. R. Lewis, R. Röttgers, A. Sciandra, M. Stramska, M. S. Twardowski, B. A. Franz, and H. Claustre. 2008. Relationships between the surface concentration of particulate organic carbon and optical properties in the eastern South Pacific and eastern Atlantic Oceans. Biogeosciences, 5, 171–201.

Stumpf, R.P., Holderied, K., Sinclair, M., 2003. Determination of water depth with high-resolution satellite imagery over variable bottom types. Limnol. Oceanogr. 48, 547–556. https://doi.org/10.4319/lo.2003.48.1_part_2.0547

Zhang, X., L. Hu, and M.-X. He. 2009. Scattering by pure seawater: Effect of salinity. Opt. Express, 17(7), 5698–5710. doi: 10.1364/OE.17.005698